



Module 6

Advanced charge exchange plasma receiver and beam donor modelling
– the current state.

Lecture viewgraphs

Hugh Summers, Luis Menchero, Martin O'Mullane and Alessandra Giunta

University of Strathclyde

Contents

1. Charge exchange data for medium weight and heavy receiver ions.
2. Extending population models for medium-weight receivers.
3. Exact Stark atom representations and field ionisation.
4. Collisions, directionality and orientation.
5. Conclusions.

1.1 Patterns of CX lines in the visible

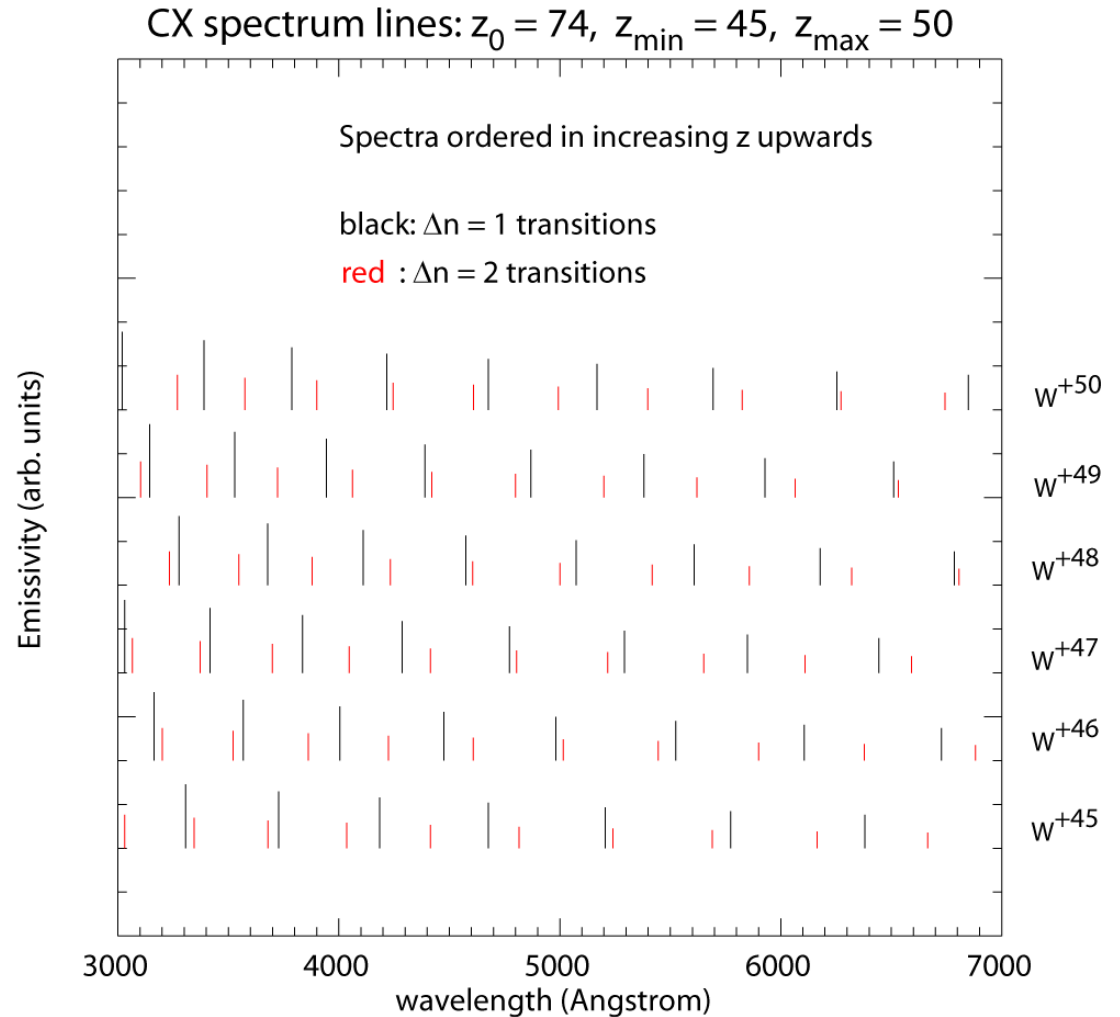
For light elements bare nucleus charge exchange receivers, up to neon, only one or two CX lines occur in the visible spectral range.

As the nuclear charge of the receiver increases, $n_{\text{crit}} \sim z_0^{3/4}$ increases. The number of lines in the visible increases and they become weaker.

The weakening of the lines means that the possibility of individual line CX spectroscopy, in the manner adopted for light elements, can only continue up to about Fe^{+26} .

With heavy elements of high nuclear charge, the partially stripped ions occur in the confined plasma, so they are also possible charge exchange receivers. By tungsten, a very large number of weak charge exchange lines are expected in the visible.

Although weak, their presence can disturb other diagnostic inferences. So it remains necessary to be able to calculate them.



1.2 Z-scaling of total CX xsects: H(1s) donor

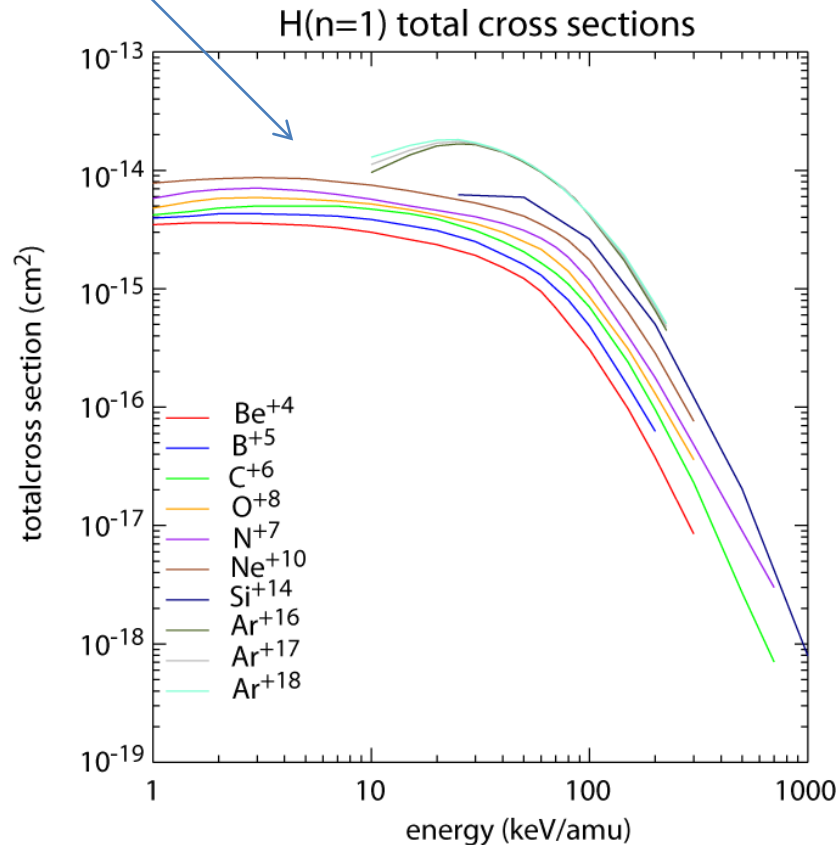
For CX capture by heavier species into higher n-shells, the receiver core is passive. Only the receiver ion charge z_1 matters. The scaling $n_{crit} \sim z_0^{3/4}$ suggests a z-scaled approach for the cross-sections.

Introduce scaled energy \bar{E} and scaled total cross-section $\bar{\sigma}_{tot}$ as:

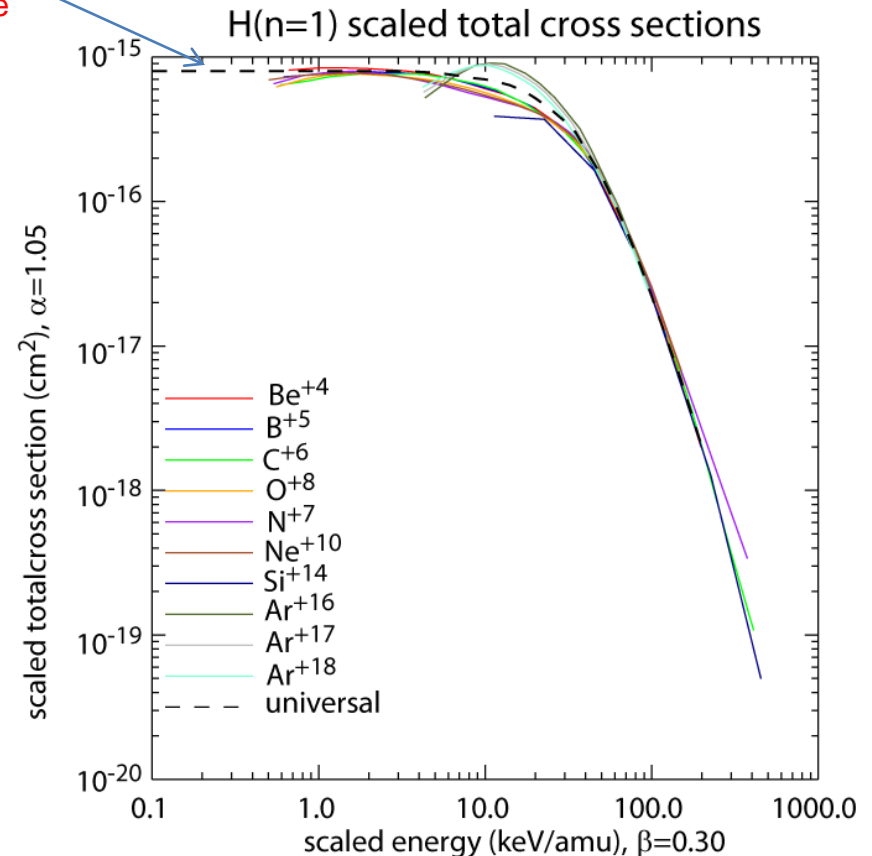
$$\bar{E} = E z_1^{-\beta} \quad \bar{\sigma}_{tot} = \sigma_{tot} z_1^{-\alpha}$$

The parameters α and β are chosen for best convergence

Results from specific calculations



Best universal curve



1.3 Z-scaling of partial-n CX xsects: H(1s) donor

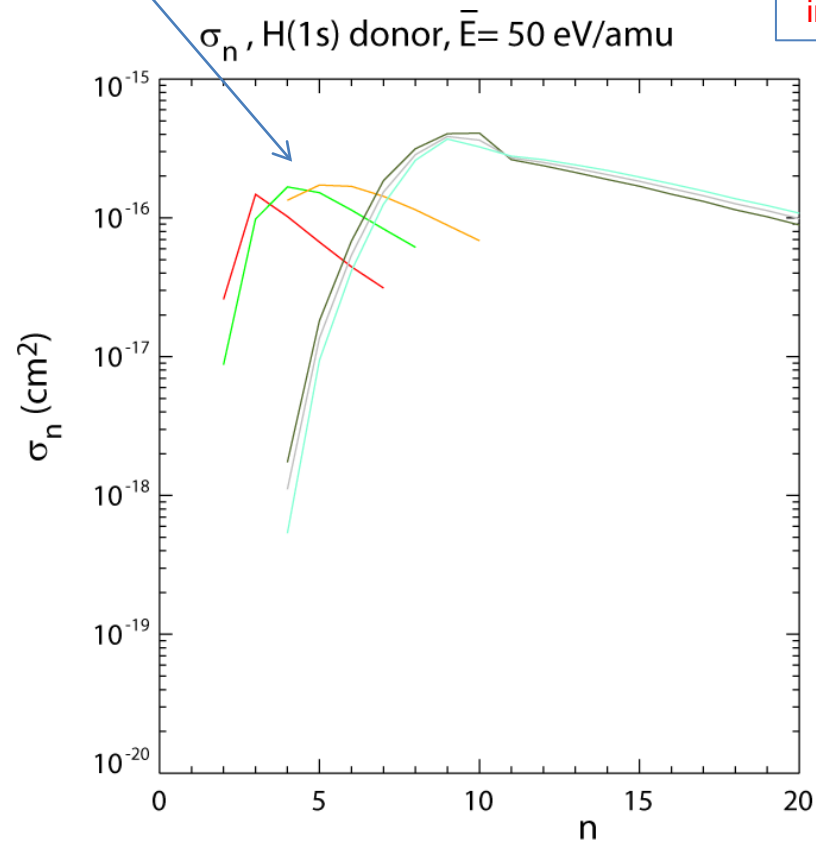
Likewise, the scaling $n_{crit} \sim z_0^{3/4}$ suggests the same approach for the partial-n cross-sections.

For each E , that is at its corresponding \bar{E} , choose z-scaling parameters γ and δ for best convergence for the different ions as:

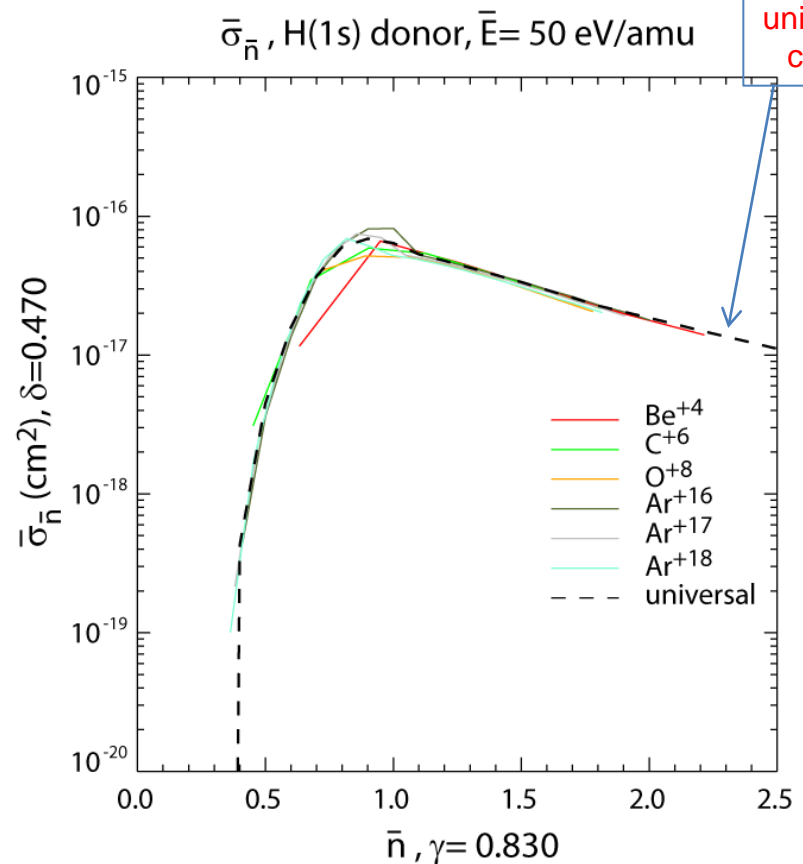
$$\bar{n} = n z_1^{-\gamma(\bar{E})} \quad \bar{\sigma}_n = \sigma_n z_1^{-\delta(\bar{E})}$$

Results from specific calculations

Note:
non-integral



Best
universal
curve



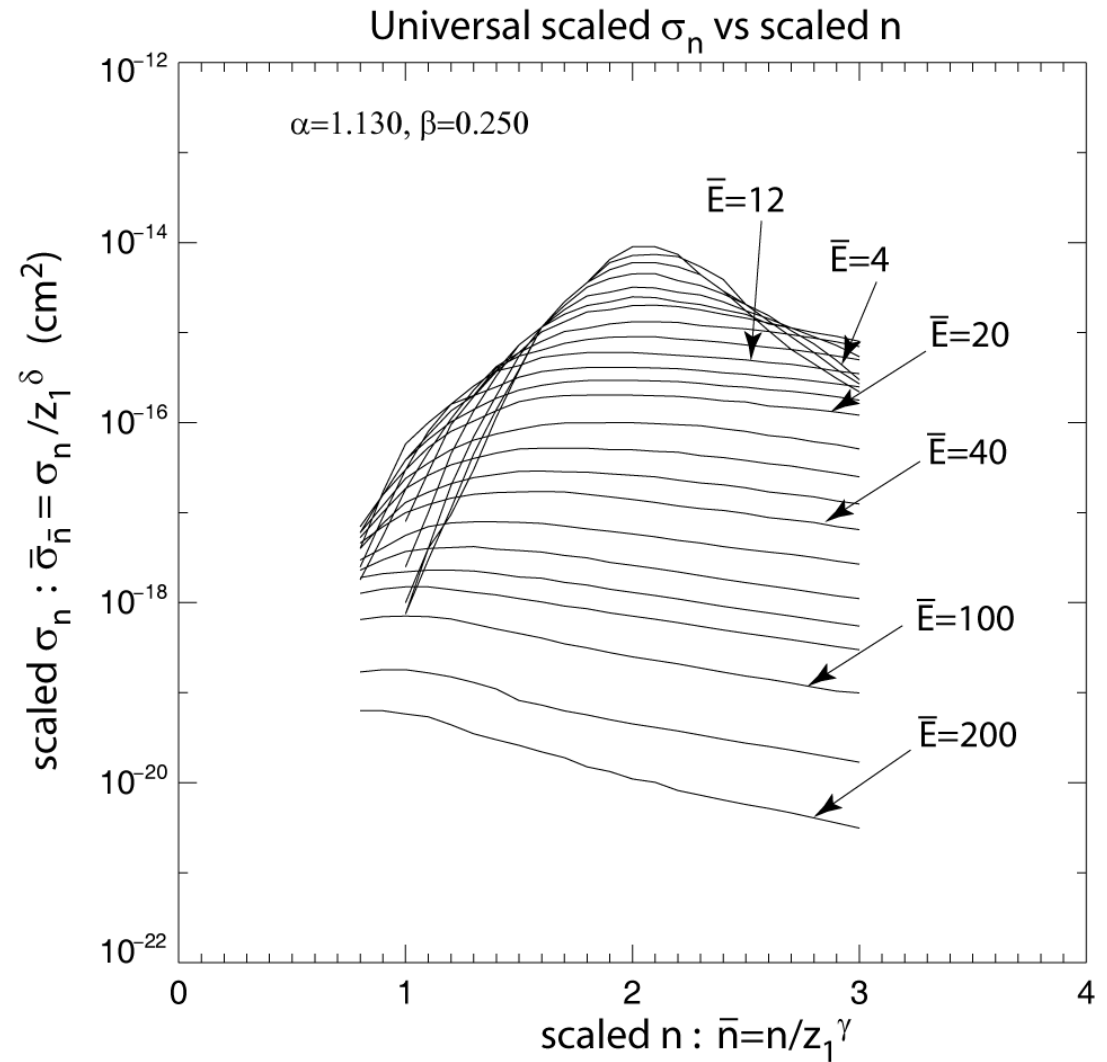
1.4 Universal scaled σ_n Vs scaled n for selected scaled E.

The scaling parameters for the final universal semi-empirical data and formulae are optimised fits to the available specific receiver ion data.

Completion of the final values require extrapolation to high n-shells outside the range of the source data using the procedures of module 5. Partial-n results are normalised to optimised total cross-sections.

The above procedure has been carried out for both H(1s) and H(2s,2p) donors.

Calculations have recently been completed for ADAS-EU including new data for B⁺⁵, N⁺⁷, O⁺⁸, Ar⁺¹⁸ and Kr⁺³⁶. A revised optimisation of the universal formula will be issued in a subsequent ADAS release.



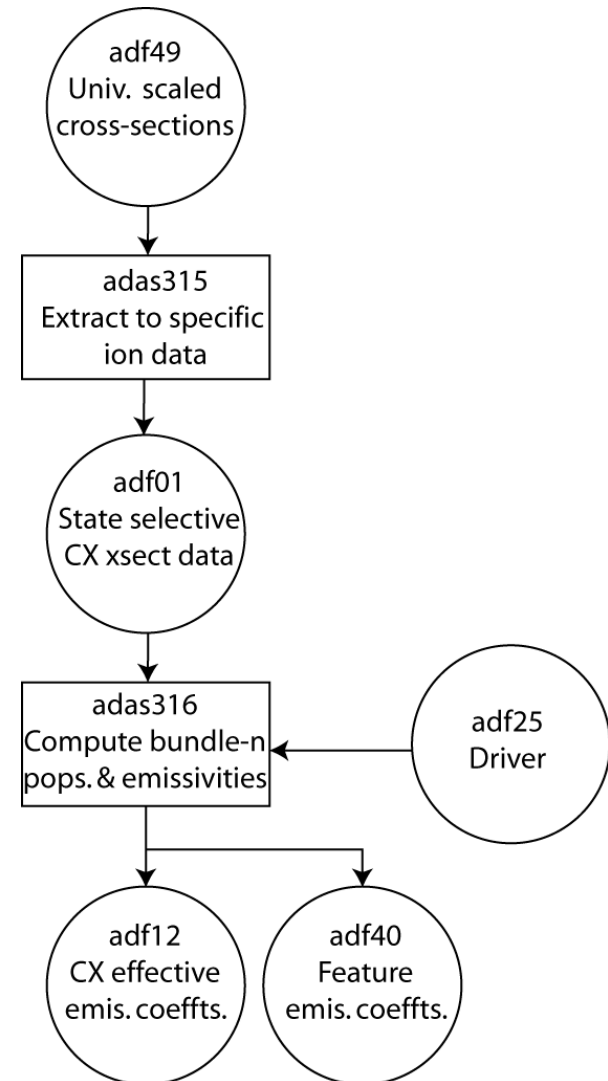
1.5 Universal scaling and heavy receiver CXS emissivities

An ADAS data format [adf49](#) has been assigned to the universal CX scaled cross-section data.

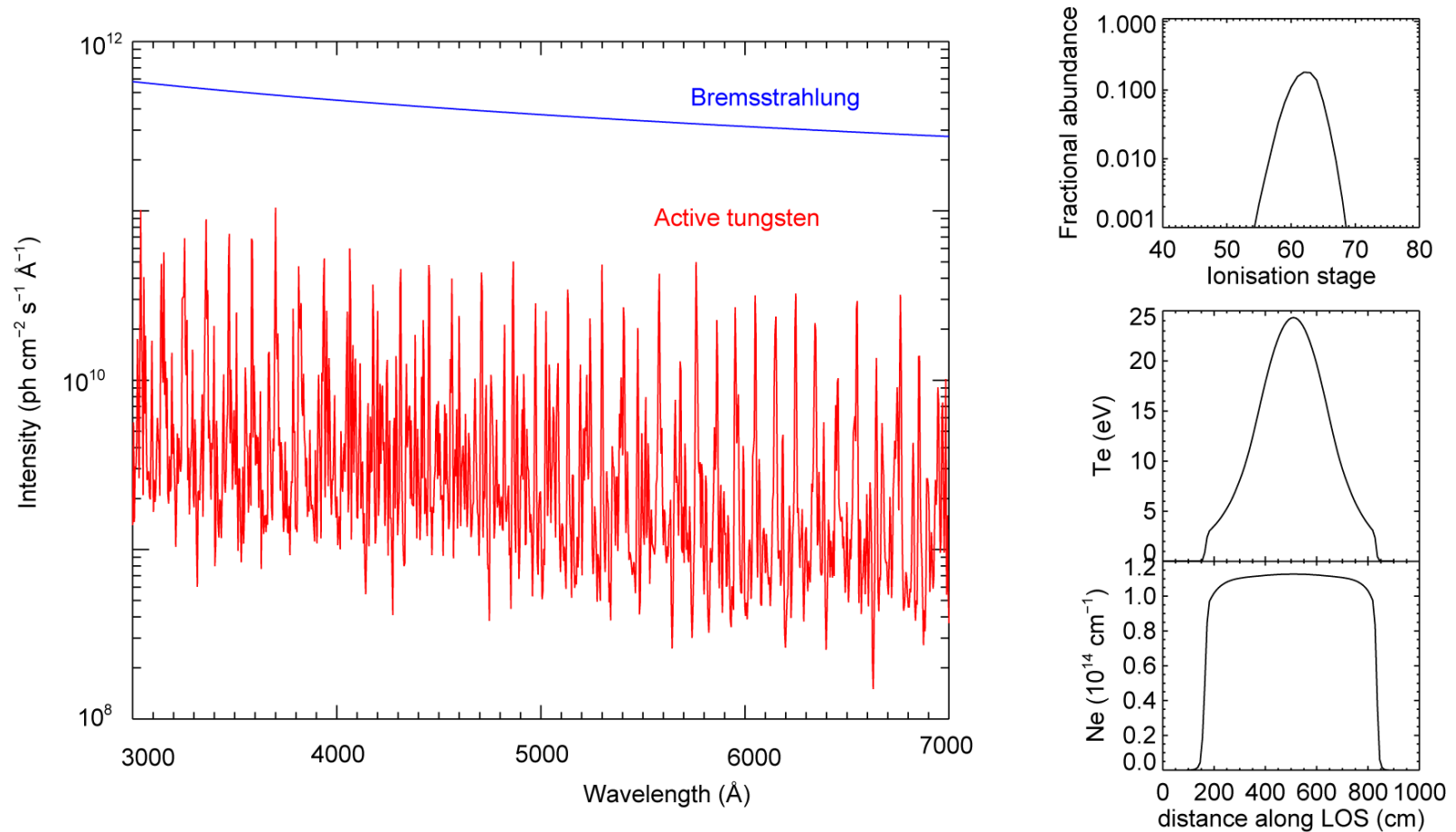
The interactive ADAS series 3 code [ADAS315](#) extracts from [adf49](#), producing a standard charge exchange cross-section dataset of format [adf01](#) for any ion (that is residual ion charge).

For heavy ion receivers, the special algorithms and codes [ADAS306](#) – [ADAS309](#) are less appropriate. Refined individual line CXS is at this point less likely. Consistency in the handling of suppression of the populations of the highest n-shells (in the collisional-radiative sense) by stepwise ionisation is important.

The processing chain to effective emission coefficients ([adf12](#) and [adf40](#)) is completed with the bundle-n population model [ADAS316](#) as shown in the schematic.



1.6 ITER: tungsten CX emission compared with Bremsstrahlung



- 50 keV/amu D beam (diagnostic NB), JNBI=300A/m², INBI=60A
- Using ITER scenario 2 (Te=24keV core, Ne=1x10¹⁴cm⁻³)
- No transport – steady state ionisation balance
- Assume looking vertically down on the beam at the core.
- No beam attenuation effects taken into account.
- W concentration = 1x10⁻⁶ of N_H

2.1 High n-shell fine structure in $(J_p)nlj$, $(J_p)nl$ and $(J_p)n$ for bundles

For the medium weight elements between argon and iron, further CXS spectroscopy may be anticipated. For these elements, the few-electron (1-6) electron receivers may be expected as well as the bare nucleus

Whereas the core of the receiver ion is of little influence on the charge exchange capture (only the residual ion charge matters), this is not so for redistribution in l -shell after capture and before emission. The fine energy separations are influential, especially towards low l .

There are four steps:

1. The precise energy levels
2. Assigning $(J_p)nlj$ quantum numbers
3. Bundling for population models
4. The population model

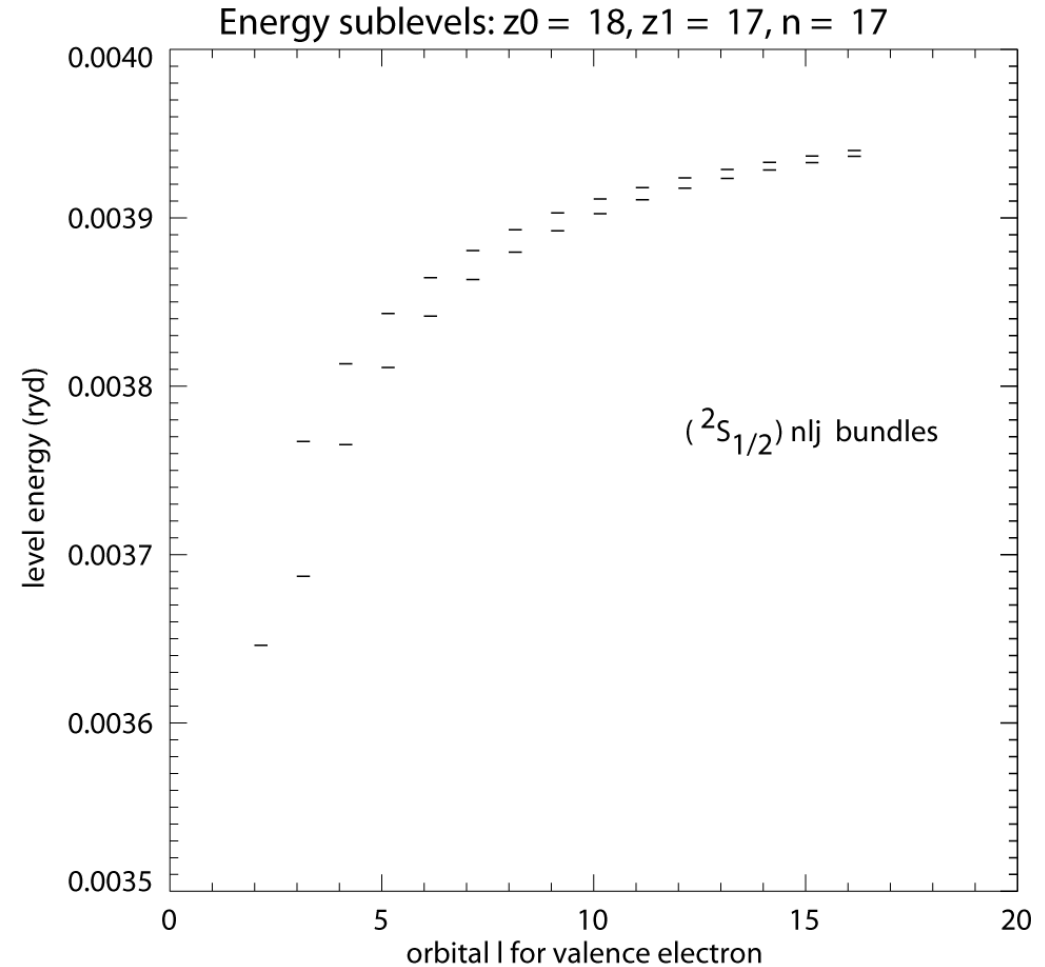
(1) **Energy levels:** Autostructure, multi-config, *ic*, scripted

$$\left[1s^2 2s^2 2p^q nl : l = 0, \dots, \min(l_{\text{cut}}, n-1) \right]$$

$$\left[1s^2 2s 2p^{q+1} nl : l = 0, \dots, \min(l_{\text{cut}}, n-1) \right]$$

$$\left[1s^2 2p^{q+2} nl : l = 0, \dots, \min(l_{\text{cut}}, n-1) \right]$$

$$\left[1s^2 2s^2 2p^q nl, 1s^2 2s 2p^{q+1} nl, 1s^2 2p^{q+2} nl \right] : l = l_{\text{cut}}, \dots, (n-1)$$



2.2 Handling medium-weight receivers in $(J_p)nlj$, $(J_p)nl$ and $(J_p)n$ bundles

- (2) **Quantum numbers:** exploits energy ordering within a symmetry rules.

Appropriate quantum numbers

$$E_{([\gamma] J_p) n l j} = \left(\sum_J (2J + 1) E_{([\gamma] J_p) n l j J} \right) / (2j + 1) \rightarrow b_{(J_p) n l j}$$

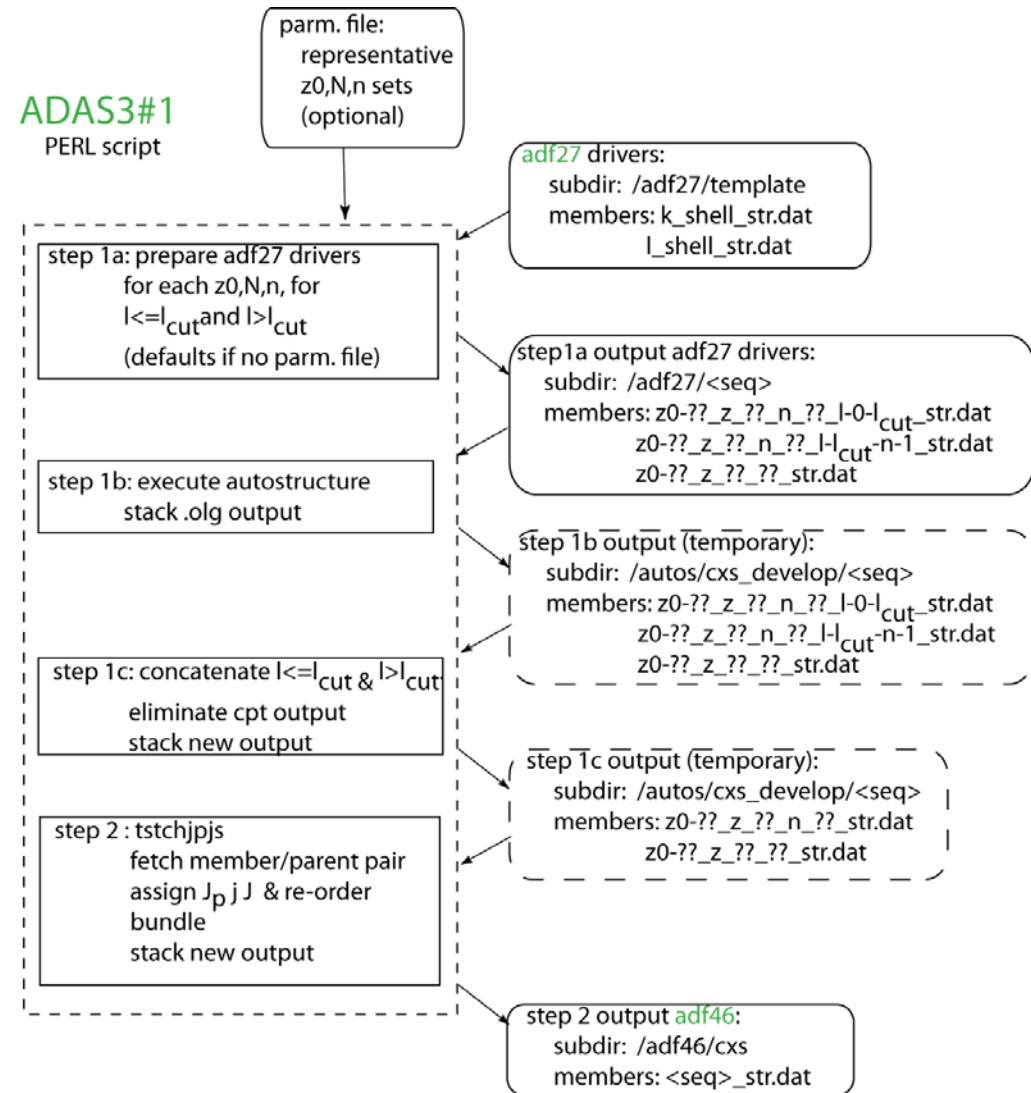
Bundles or population models

$$E_{([\gamma] J_p) n l} = \left(\sum_{j=l-1/2}^{j=l+1/2} (2j + 1) E_{([\gamma] J_p) n l j} \right) / 2(2l + 1) \rightarrow b_{(J_p) n l}$$

$$E_{([\gamma] J_p) n} = \left(\sum_l (2l + 1) E_{([\gamma] J_p) n l} \right) / 2n^2 \rightarrow b_{(J_p) n}$$

ADAS316

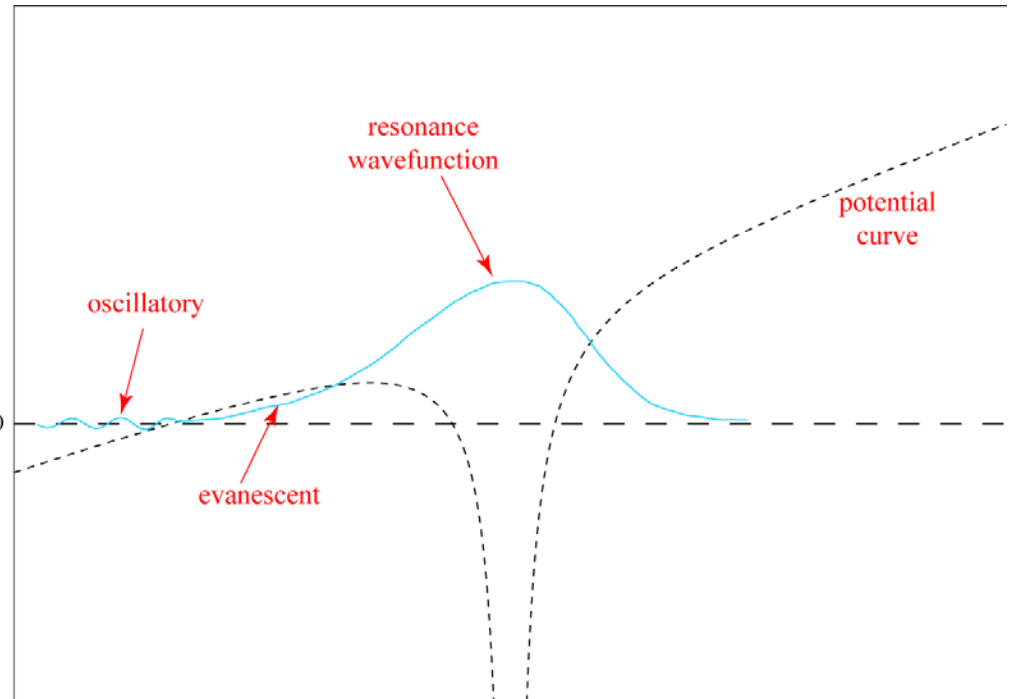
ADAS317 being brought back into use for this purpose with additions



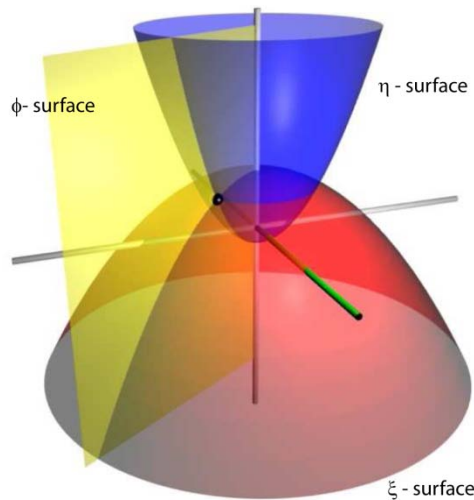
3.1 Stark state – resonance character

Although a hydrogen atom state in a Stark field is often treated as a bound state, its wave-function is non-vanishing at infinity on the low-field side. Properly it is a *resonance* embedded in a continuum sea.

In the simpler viewpoint, it is argued that the bound electron can tunnel through the potential barrier in -ve z-direction, resulting a *field ionisation rate*. Also the energy levels of the Stark atom are calculated as a 1st order perturbation of the isolated atom.



Working in parabolic coordinates



$$\begin{aligned}
 x &= \sqrt{\xi\eta} \cos \phi \\
 y &= \sqrt{\xi\eta} \sin \phi \\
 z &= \frac{\xi - \eta}{2} \\
 r &= \frac{\xi + \eta}{2}
 \end{aligned}$$

The Hamiltonian is

$$H = -\frac{2}{\xi + \eta} \frac{\partial}{\partial \xi} \left(\xi \frac{\partial}{\partial \xi} \right) - \frac{2}{\xi + \eta} \frac{\partial}{\partial \eta} \left(\eta \frac{\partial}{\partial \eta} \right) - \frac{1}{2\xi\eta} \frac{\partial^2}{\partial \phi^2} - \frac{2}{\xi + \eta} + \frac{1}{2} F (\xi - \eta)$$

Electric field strength



3.2 The complex coordinate rotation

By a rotation in the complex plane through a variable angle ϑ as $r' = r e^{i\vartheta}$ the resonant states and their character may be determined.

The Hamiltonian in the rotated coordinate is no longer Hermitian and its eigenvalues are complex.

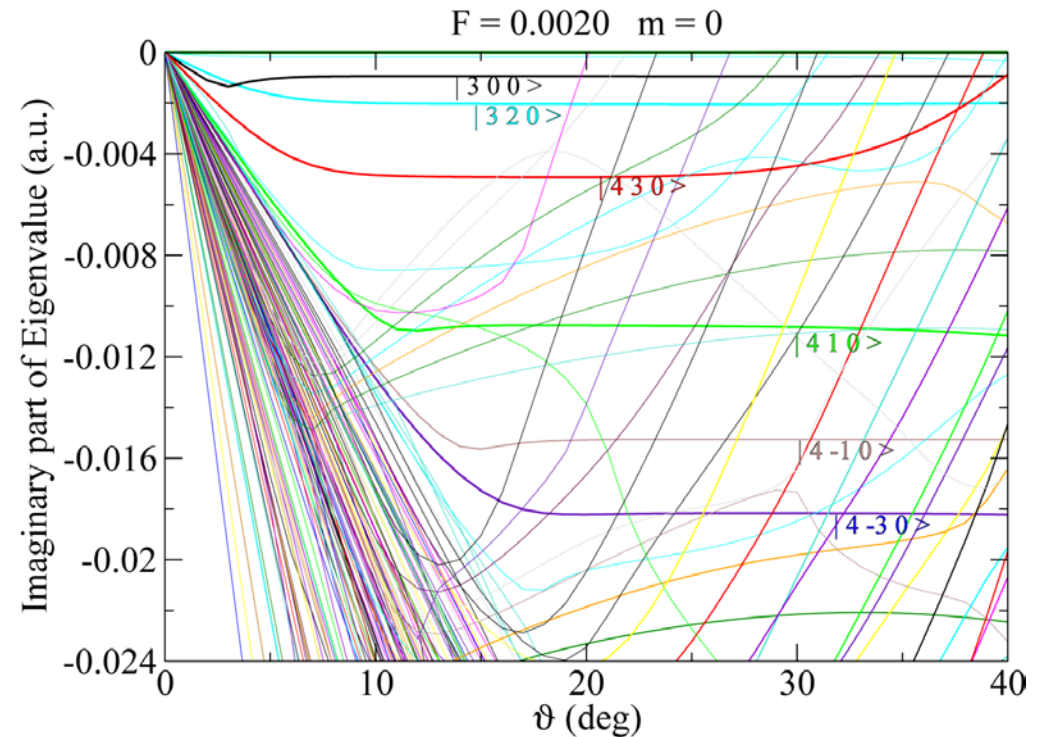
There are three types of effect of the transformation on the eigenvalues:

- bound states are unchanged
- continuum branches are rotated at an angle 2ϑ with the real axis with origin at the threshold energy.
- resonances are exposed in the complex plane when the rotation angle ϑ is greater than the complex root of the resonance.

Let the complex energy of the resonance be:

$$E = E_r - i \frac{\Gamma}{2} = |E| e^{i\beta}$$

$$E_r$$



The figure shows the resonances being exposed as the angle ϑ is varied against the continuous background. Their trajectories become horizontal when the angle ϑ is greater than the argument β .

3.3 Solving the secular equation, the Laguerre basis and matrix handling

Expand the wavefunction in a basis set separating the coordinate variables ξ and η as:

$$\Psi(\xi, \eta, \varphi) = \frac{1}{\sqrt{2\pi}} e^{im\varphi} \sum_{k=1}^N \sum_{l=1}^N c_{klm} g_k(\xi) g_l(\eta)$$

The Hamiltonian becomes

$$\begin{aligned} H_{klk'l'm}(\vartheta) &= \langle g_k g_l | H(\vartheta) | g_{k'} g_{l'} \rangle \\ &= \int_0^\infty d\xi \int_0^\infty d\eta \frac{1}{4} (\xi + \eta) g_k^*(\xi) g_l^*(\eta) H(\vartheta) g_{k'}(\xi) g_{l'}(\eta) \\ &= -\frac{e^{-2i\vartheta}}{2} (\mathcal{T}_{kk'} \mathcal{I}_{ll'} + \mathcal{I}_{kk'} \mathcal{T}_{ll'}) - \frac{e^{-i\vartheta}}{2} \mathcal{I}_{kk'} \mathcal{I}_{ll'} + \frac{e^{i\vartheta}}{8} F (\mathcal{F}_{kk'} \mathcal{I}_{ll'} - \mathcal{I}_{kk'} \mathcal{F}_{ll'}) \end{aligned}$$

and the overlap integral become

$$\begin{aligned} S_{klk'l'm} &= \langle g_k g_l | g_{k'} g_{l'} \rangle \\ &= \int_0^\infty d\xi \int_0^\infty d\eta \frac{1}{4} (\xi + \eta) g_k^*(\xi) g_l^*(\eta) g_{k'}(\xi) g_{l'}(\eta) \\ &= \frac{1}{4} (\mathcal{S}_{kk'} \mathcal{I}_{ll'} + \mathcal{I}_{kk'} \mathcal{S}_{ll'}) \end{aligned}$$

leading to solution of the secular equation matrices $\mathcal{T}_{kk'}$, $\mathcal{F}_{kk'}$ and $\mathcal{I}_{kk'}$.

$(\mathbf{H} - \mathbf{E}\mathbf{S})\mathbf{C} = 0$ efficiently for any F and ϑ in terms of the

In practice, a finite basis of Laguerre mesh polynomials is used as:

$$\Lambda_{Ni}(x) = (-1)^i \sqrt{x_i} \sum_{j=0}^{N-1} \frac{(-1)^{j+1}}{(j+1)!} L_{N-j-1}^{j+1}(x_i) (x - x_i)^j$$

3.4 Stark state wave functions in ξ , η space

States are labelled $|\tilde{n} \tilde{k} m\rangle$ with the approximate quantum numbers \tilde{n}_1 and \tilde{n}_2 which correspond to the quasi-nodes of the modulus of the partially integrated wavefunctions.

$$\psi_\xi(\xi) = \int_0^\infty d\eta \psi(\xi, \eta)$$

$$\psi_\eta(\eta) = \int_0^\infty d\xi \psi(\xi, \eta)$$

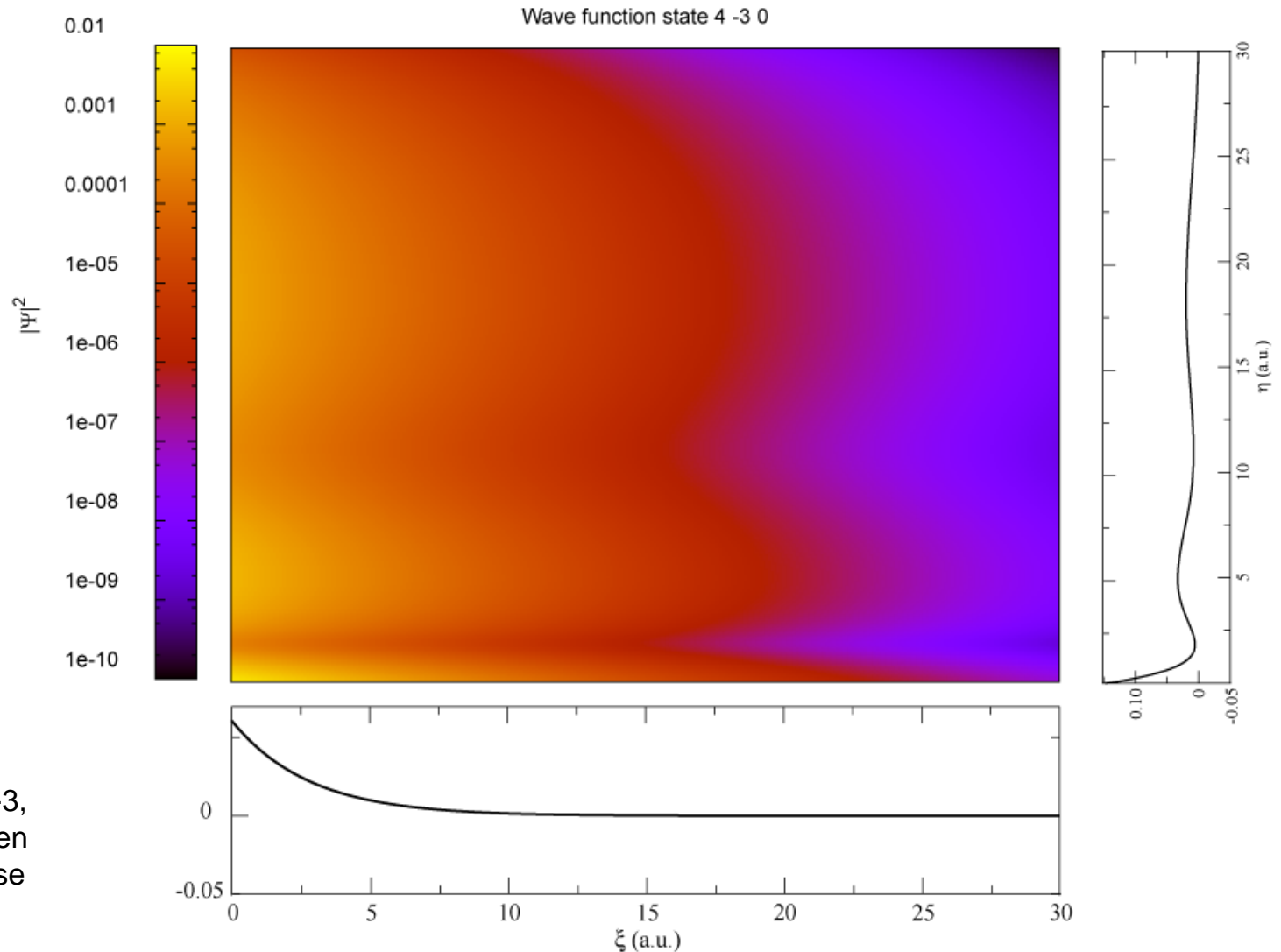
Note that

$$\tilde{n} = \tilde{n}_1 + \tilde{n}_2 + |m| + 1$$

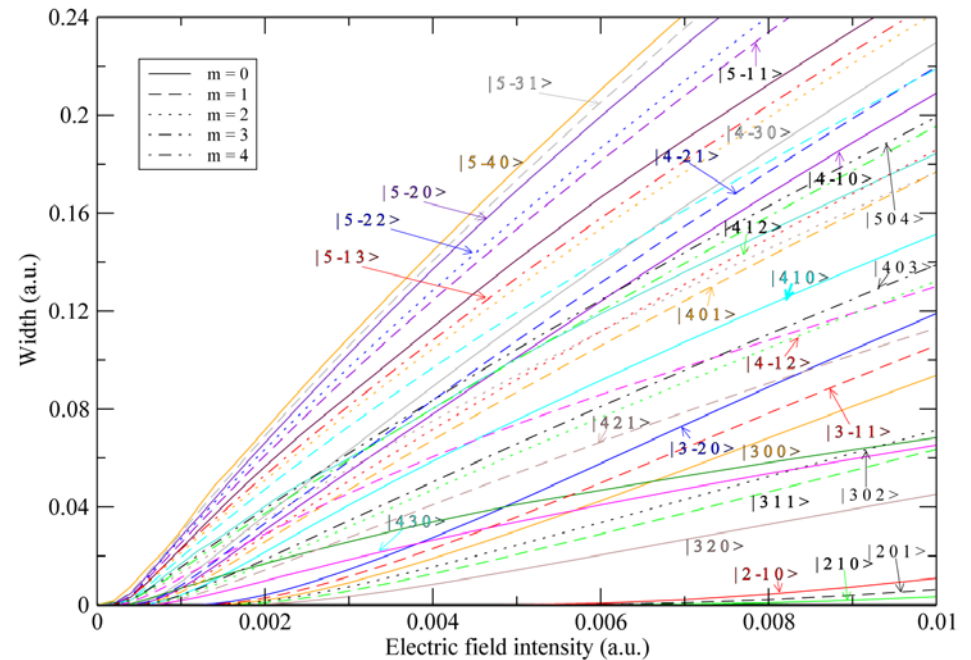
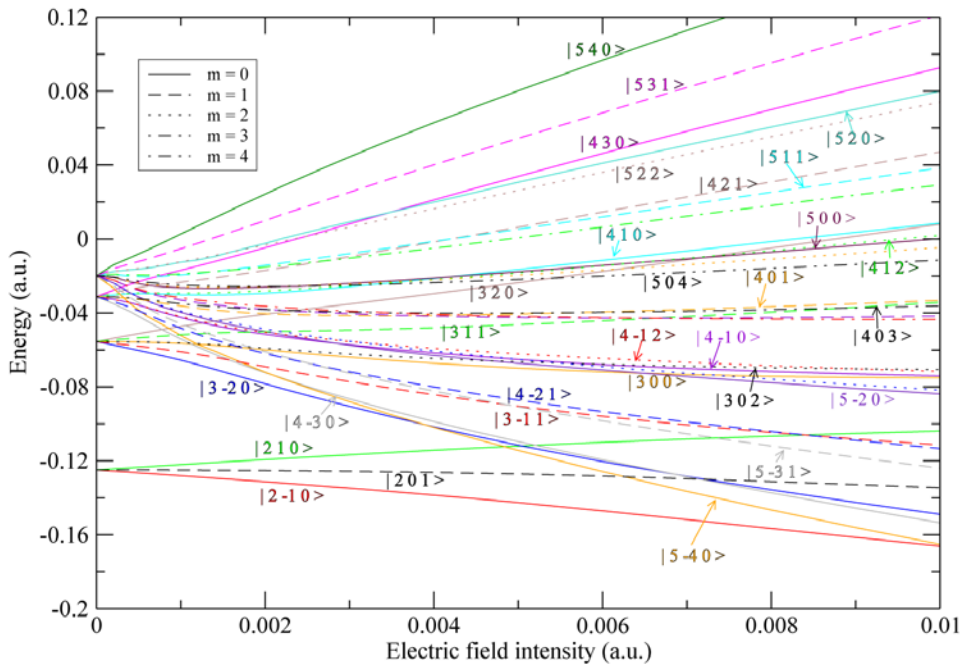
$$\tilde{k} = \tilde{n}_1 - \tilde{n}_2$$

\tilde{k}

The figure is of the $n=4$, $k=-3$, $m=0$ wavefunction. For given n , the level energies increase with increasing k .



3.5 Energies and widths



Energies of the resonances up to $n=5$ for the hydrogen atom vs electric field strength. Note that: 0.01 a.u. = 5.1×10^9 V/m.

Widths of the resonances up to $n=5$ for the hydrogen atom vs electric field strength. Note that: 0.01 a.u. = 5.1×10^9 V/m.

The solution above together with its archive of the matrix elements and others required for transition probabilities, angular momentum, Runge-Lenz etc. permits a return to the code [ADAS305](#) described in [module 5](#). Now only secondary interactions due to magnetic moment and minor electric fields are treated in 1st order perturbation theory.

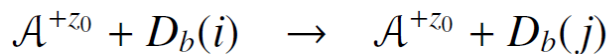
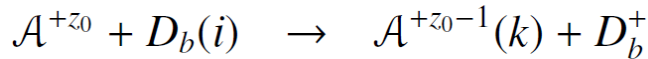
The revision of [ADAS305](#), to be called [ADAS316](#), is in progress. Useful fundamental atomic data such as the energies, widths (field ionisation lifetimes) and A-values are being archived in format [adf50](#).

4.1 Ion and electron collisions with neutral beam atoms

In the core plasma $|\vec{v}_e - \vec{v}_{beam}| \sim v_e$ where \vec{v}_e represents a mean thermal electron velocity, whereas $|\vec{v}_i - \vec{v}_b| \sim v_b$ where \vec{v}_i represents a mean thermal ion velocity. Thus electron collisions are effectively isotropic but ion collisions are not. \vec{v}_b is the beam velocity.

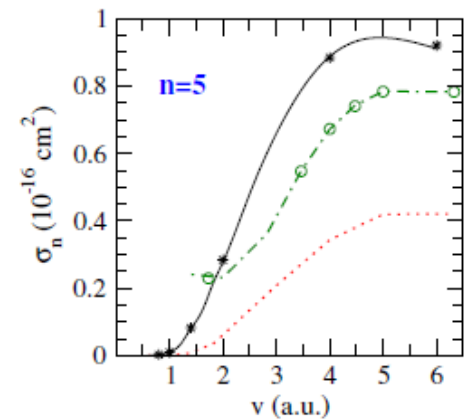
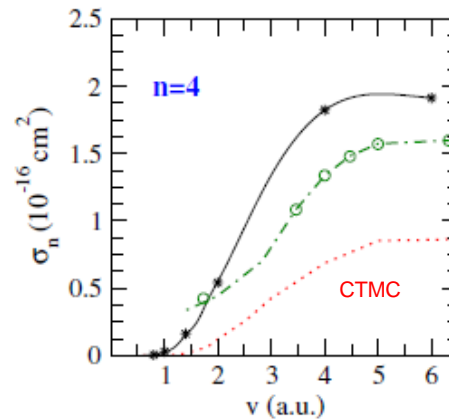
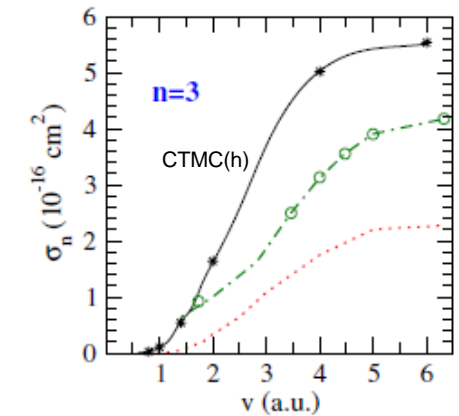
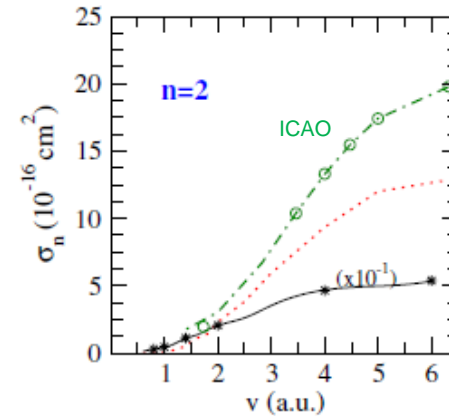
Because of the speed of the beam and electrons in the thermal core of the plasma, electron-impact collision cross-sections for beam-atom excitation are generally much smaller than ion-impact cross-sections.

For ion collisions with beam atoms, the charge transfer and beam excitation reactions are complementary.



Both should be evaluated consistently in the one close-coupled calculation. This is often not done.

The recent calculations of B (CCMO), N, O and Ar (CCAO) for state selective charge transfer cross-sections do not include the beam atom excitation cross-sections. On the other hand the CTMC improved calculations for Ne, Ar and Kr do. The latter can **act as a basis for a universal approximation** similar to charge transfer.



4.2 Impact parameter approaches

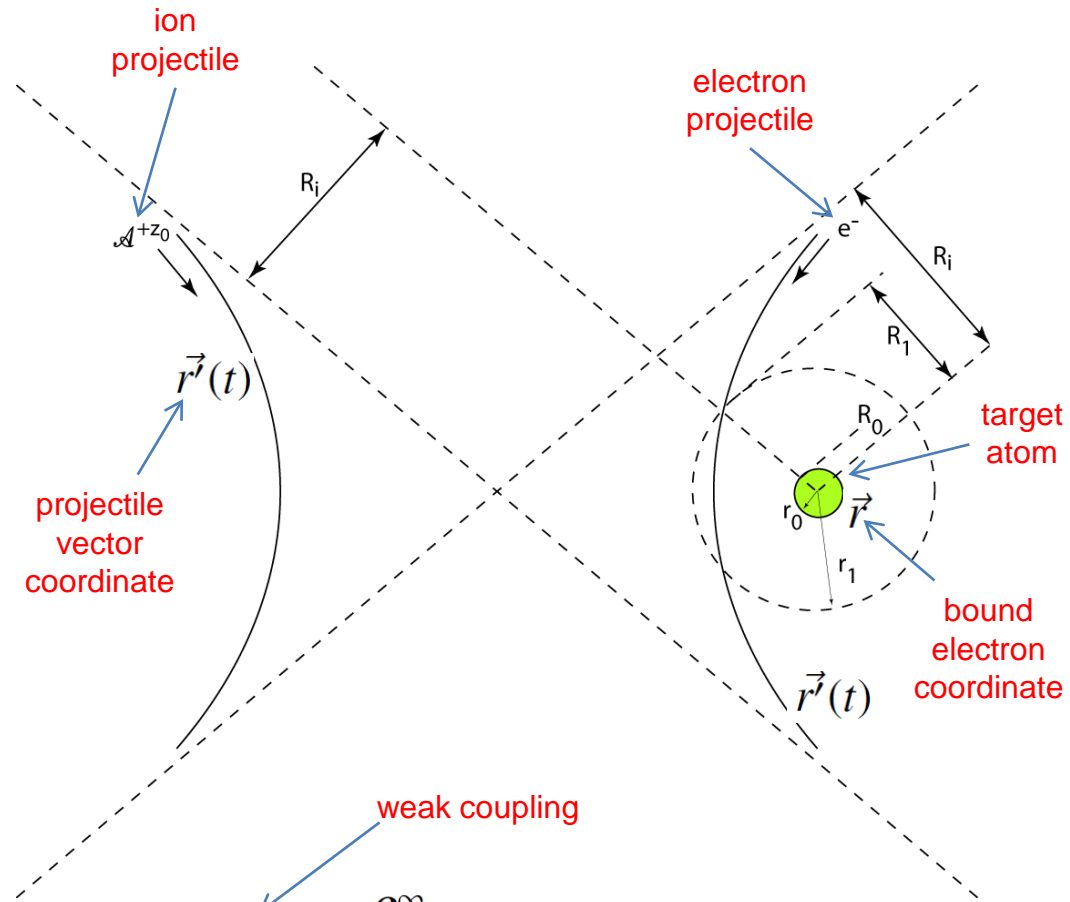
The treatment of the collider as travelling on a classical trajectory is frequently used in atomic collision physics. It has wide validity for ion colliders and is useful for electron collisions.

The trajectory is hyperbolic (attractive or repulsive for electron or ion respectively) if both projectile and target are charged (as shown in the schematic), otherwise it is a straight line. The latter is the situation for excitation of neutral beams.

The probability of inducing the transition i to j in the target by a collider on the trajectory of impact parameter R_i is $P_{ij}(R_i)$. Then the cross-section is

$$Q(i \rightarrow j) = \int_0^\infty P_{ij}(R_i) 2\pi R_i dR_i$$

Considerations of whether the trajectory penetrates the atom, R_0 , or if the probability exceeds $\frac{1}{2}$, R_1 , leads to so-called **weak coupling** and **strong coupling** versions of the cross-section. Simplified approximations for those are shown on the right.



$$Q_W(i \rightarrow j) = \int_{R_0}^\infty P_{ij}(R_i) 2\pi R_i dR_i$$

$$Q_S(i \rightarrow j) = \frac{1}{2} \pi R_1^2 + \int_{R_1}^\infty P_{ij}(R_i) 2\pi R_i dR_i$$

4.3 Working with path integrals

The probability of transition from time-dependent perturbation theory is

$$P_{ij} = \frac{1}{\hbar^2 \omega_i} \left| \int_{-\infty}^{+\infty} e^{ipt} V_{ij}(t) dt \right|^2$$

with the interaction potential

$$V_{ij} = \int \phi^*(\vec{r}) \frac{e^2}{|\vec{r}'(t) - \vec{r}|} \phi(\vec{r}) d^3 \vec{r}$$

This can be expanded in multipoles, most simply retaining only the dipole term and assuming no penetration of the collider closer to the nucleus than the bound electron. With these restrictions and assuming an orbit in the x-y plane, P_{ij} is expressible in terms of two path integrals which yield modified K Bessel functions. In the isotropic case

$$P_{i \rightarrow j} = 4 \left(\frac{I_H}{\Delta E_{ij}} f_{i \rightarrow j} \right) \frac{k_i k_j}{(k_i k_j R_c + z z' / a_0)^2} X(\xi, \delta)$$

$$X(\xi, \delta) = \exp(\pi \xi) (\xi \epsilon)^2 \left[K'_{i\xi}{}^2(\xi \epsilon) + \frac{\epsilon^2 - 1}{\epsilon^2} K_{i\xi}^2(\xi \epsilon) \right]$$

$$\text{and } \xi = \frac{z z'}{a_0} \left| \frac{1}{k_i} - \frac{1}{k_j} \right| \quad \delta = R_c |k_i - k_j|$$

$$\text{with } \delta = \xi \epsilon - \xi.$$

ADAS has subroutines for these cross-sections and related functions [eiqip.for](#), [xip.for](#), [yip.for](#) together with many other cross-section approximations.

The form and evaluation of the path integrals has been used to handle degenerate transitions, allow penetration of the atom, include higher multipoles and so on. **It is an active area at this time.**

In the present context of collisional excitation and re-distribution of fast beam atoms, the ADAS team is testing these methods for the **oriented Stark atom**, experiencing **highly directional collisions**.

4.4 Directional and orientation issues

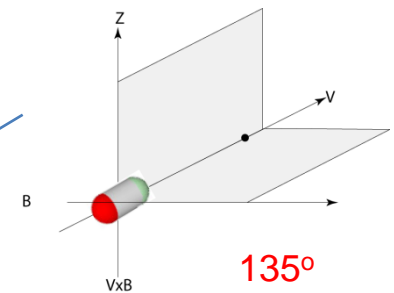
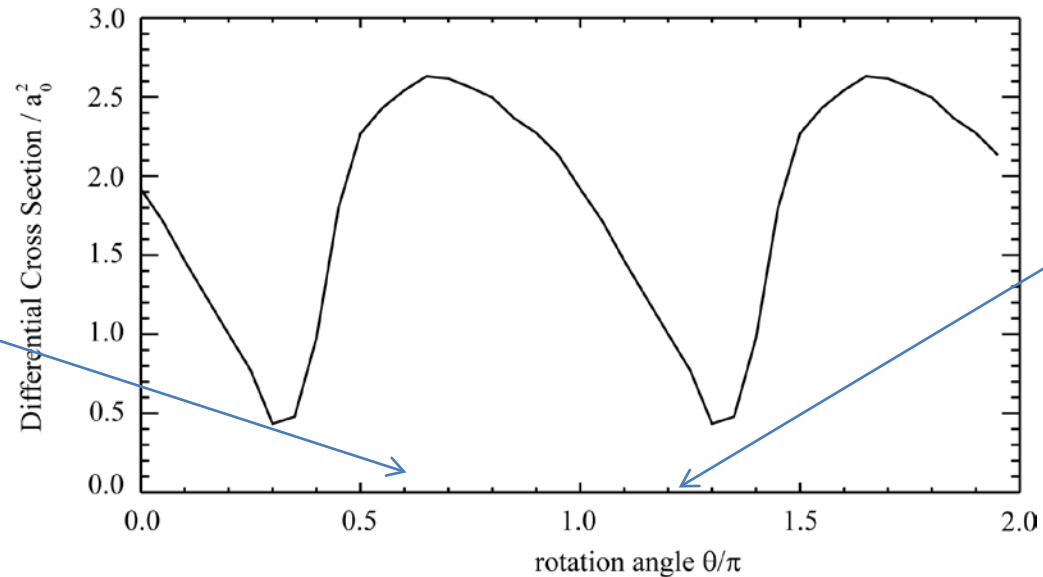
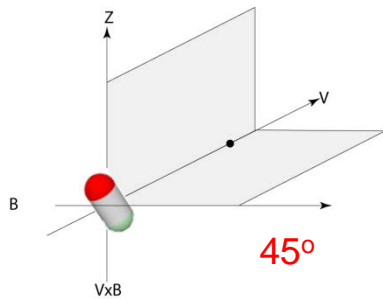
The probability generalises in the directional/ oriented case requires the **three component path integrals** and three matrix elements between **Stark states**.

$$P_{s \rightarrow s'} = \frac{e^4}{(4\pi\epsilon_0)^2 \hbar^2} \left| \int_{-\infty}^{\infty} \exp(i\Delta E_{s,s'} t / \hbar) \left(\frac{x'(t)}{r'^3(t)} \langle \psi_s | x | \psi_{s'} \rangle + \frac{y'(t)}{r'^3(t)} \langle \psi_s | y | \psi_{s'} \rangle + \frac{z'(t)}{r'^3(t)} \langle \psi_s | z | \psi_{s'} \rangle \right) dt \right|^2$$

The cross-section is an integral over the **cone of attack** and the strong coupling circle is now a more complex area

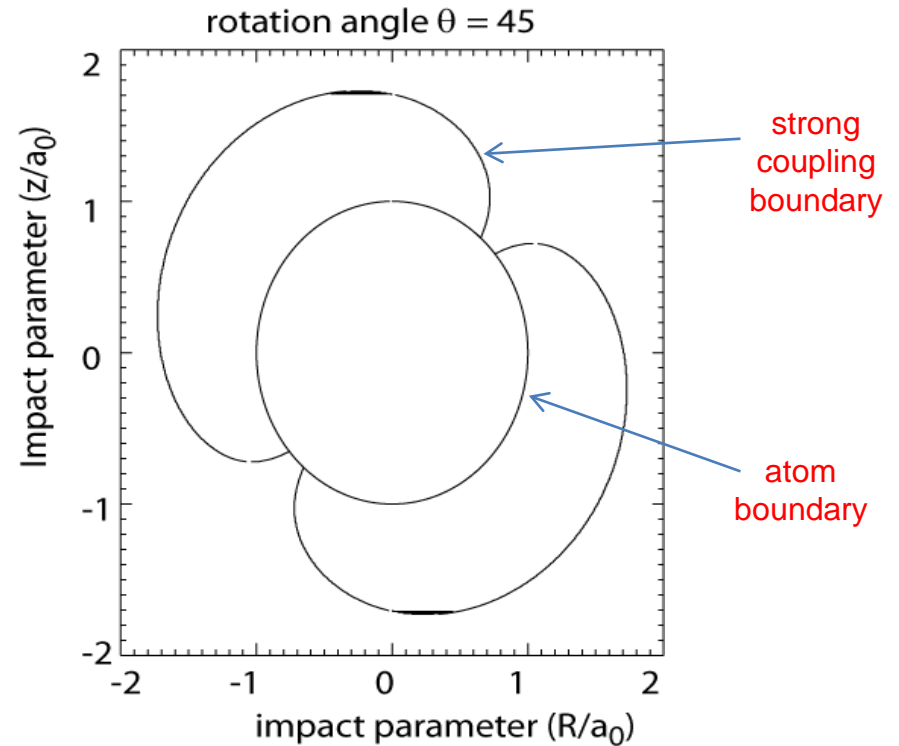
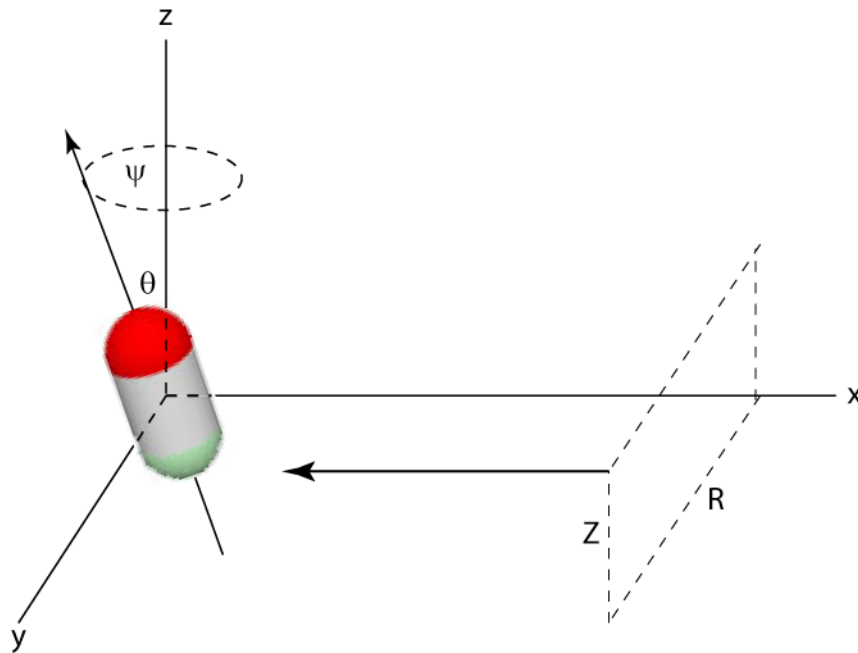
$$Q_{i\sigma j\eta}^{tot} = \frac{1}{2\pi\theta_0} \int_0^{\theta_0} \left[A(\vec{r}_1, \theta) + \int_0^{2\pi} \int_0^{\infty} \int_{R_1}^{\infty} (P_{i\sigma j\eta}(\theta, \psi, Z, R) dR dZ d\psi) \right] \sin\theta d\theta$$

The schematic and an illustrative graph below shows the broad type of behaviour.



4.5 Strong coupling zones

The shape of the strong coupling area is illustrated below with a schematic of the impact parameters.



The brief discussion above summarises **work in progress** for the neutral beam description, utilising the zeroth order Stark states and matrix elements evaluated in section 4. The cross-sections will be normalised at zero field in the isotropic case to the CTMC (h) data of viewgraph 5.1.

5.1 Conclusions

- The database of state selective charge transfer from H(n=1) and H(n=2) donors to fully ionised impurity nuclei up to argon has allowed preparation of a universal semi-empirical approximation for all charged receivers.
- Current utilisation for derived effective emission is through the b_n -model.
- New state selective charge transfer data, calculated for ADAS-EU confirms the broad behaviour, although some ambiguity on l-shell capture remains, and extends the available data to krypton. The universal approximation is being re-optimised using these data.
- More precise high nl-shell energies allows more precise l-distribution modelling for medium-weight partially ionised receivers. This is being enabled in the b_{nl} -model.
- Exact solutions of the motional-Stark modified beam atom have been prepared, yielding field ionisation and other quantities at high precision for arbitrary field strengths. They are being embedded in a revised beam emission model.
- Directional ion and electron collisions with the oriented Stark beam atom have been addressed in the impact parameter formalism. Modified cross-sections will be incorporated in the revised beam emission model.